Progress In Electromagnetics Research C, Vol. 118, 43–59, 2022

Ultra-Wideband Reflectarray Antenna Using Two Layers Square-Loop Frequency Selective Surfaces

Ali Mohammad* **and Ali Hassan**

Abstract—This paper aims to design an ultra-wideband reflectarray using True Time Delay technique that depends on compensation for the path differences of the electromagnetic waves between the feed and reflectarray surface, and reradiate them in-phase as a planar wave. The reflectarray surface is composed of numerous radiating elements. The reflecting surface is divided into several concentric annular zones; each of them has equal path delays of the electromagnetic waves. The radiating elements in each zone are implemented with two-layer square-loop type Frequency Selective Surface (FSS) structures. A TTD reflectarray with a diameter of 250 mm fed with a centered ku-band pyramidal horn antenna is studied, designed, and fabricated to operate at the center frequency of 15 GHz. The proposed reflectarray provides a gain of 26.42 ± 2 dB in the 12–18 GHz range achieving a fractional bandwidth of 40%. The simulated radiation patterns are stable with cross-polarization level below -40 dB and side-lobes level below -15 dB over the entire operating frequency range. The simulated phase efficiency is about 56% at the center frequency of 15 GHz.

1. INTRODUCTION

Parabolic antenna was one of the first large antennas that used in long distance communication such as satellites and radars due to its high gain and large bandwidth limited just in the bandwidth of the feed antenna [1]. However, the 3D structure, bulky size, large weight, and the difficulty of manufacturing paved the way for another type of large antennas, which is array antenna [1, 2] that consists of numerous small antennas (radiating elements) thoughtfully arranged and connected to a feed network to get high gain. However, this kind of antennas suffers from feed network complexity and the resonance behavior of the antenna elements that causes a narrow bandwidth.

Over the past decade, a new type of high gain antennas with a spatial feed — referred to as reflectarray antenna (RAA) — has aroused the interest of researchers due to its attractive design features such as light weight, ease of manufacturing, flat structure, and its dependence on spatial feed instead of complex feed network [1, 3].

The reflectarray antenna is a flat array of radiating elements designed with printed circuit technology, with a centered or shifted source of electromagnetic waves (a horn antenna usually) [3]. The radiating elements are designed to reflect the waves coming from the source in such a way that the path differences of these waves are compensated. As a result, a focused beam with high gain and narrow beamwidth is formed in the far field of the reflectarray. The configuration of the reflectarray with a feed antenna is shown in Figure 1 [3].

The limited bandwidth of reflectarray antennas is the biggest challenge for the researchers in this field. This limitation is mainly produced from the resonance behavior of the radiating elements on one hand, and the path differences of the electromagnetic waves from the feed to the radiating elements on the other hand.

Received 5 December 2021, Accepted 17 January 2022, Scheduled 27 January 2022
* Corresponding author: Ali Mohammad (ali.mohammed@hiast.edu.sy).
The authors are with the Communication Department, HIAST, Damascus, Syria.

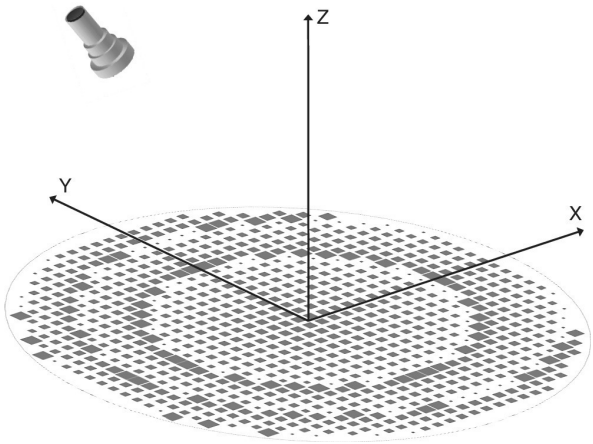

Figure 1. Configuration of the reflectarray antenna.

Over the past few years, a new type of wideband reflectarrays designed using the Frequency Selective Surfaces (FSS) is studied [4]. Frequency Selective Surfaces are an array of resonant elements — referred to as unit cells — arranged periodically, thus, the entire periodic structure can be studied and designed by studying and designing the unit cell in terms of its shape, dimensions, and number of layers [5]. The FSS idea can be used to address the problem of the resonance behavior of the radiating elements, by either designing multi-layer unit cells which leads to obtaining a multi-resonant behavior of the radiating elements and thus increasing its bandwidth [6–8], choosing complex shapes of the single-layer unit cells which also leads to obtaining a multi-resonant behavior of the radiating elements [9–13], or designing sub-wavelength unit cells, hence, a resonant coupling is obtained between the near elements [14–17]. A number of solutions have been presented to address the problem of the path differences of the electromagnetic waves from the feed to the radiating elements such as using True Time Delay (TTD) technique which depends on adding transmission lines with different lengths to compensate the path differences [18–20], or using Multi-faceted configurations which depends on folding the reflectarray aperture to compensate the path differences [21]. In [19], a TTD reflectarray antenna with sub-wavelength elements was designed in the [8–12 GHz] frequency range, but the method for getting a linear phase of the reflection coefficient from the equivalent circuit was not clear. In [20], a TTD reflectarray antenna was designed in the [8–12 GHz] frequency range, but the selected FSS configuration (dog-bone type) is not symmetric, and thus the results in E and H planes were different.

In this paper, we present a mathematical methodology for designing an ultra-wideband true-time-delay reflectarray antenna. The proposed reflectarray is composed of numerous radiating elements with different dimensions arranged on several concentric annular zones on the reflectarray aperture. Each radiating element is a two-layer unit cell of a square-loop frequency selective surface implemented on an FR4 substrate with a thickness of 0.33 mm. The square-loop FSS is a symmetric configuration, hence, the reflectarray works well in both E and H planes. The equivalent circuit model of the square-loop configuration is extracted, and the relations between the electrical and physical models are studied to compute the physical dimensions of the radiating elements in each layer and each zone. A TTD reflectarray with a diameter of 250 mm fed with a centered ku-band pyramidal horn antenna is studied and designed to operate at the center frequency of 15 GHz.

The added value of this research compared to previous researches is the reduction of the complexity and cost of the proposed design, yet obtaining very good radiation specifications. The proposed reflectarray antenna was designed using a simple symmetrical FSS configuration, with a smaller number of core cells, and using a low-performance dielectric substrate (FR4).

2. THE MAIN PARAMETERS OF THE PROPOSED REFLECTARRAY

In this section, we present the first group of design parameters that relates directly to obtaining the best reflectarray efficiency, and thus the best reflectarray gain. The efficiency of the reflectarray antenna is

the ratio of the radiated power from the reflectarray antenna to the total power provided by the feed antenna, thus it is mainly related to the following parameters: the specifications of the feed antenna, the shape of the reflectarray aperture, the focal ratio F/D which is defined as the ratio of the distance between the feed antenna and the surface of the reflectarray to the diameter of the reflectarray, and the wave properties at the edge of the reflectarray, expressed by the edge taper or edge diffraction parameter.

The specifications of the feed antenna are one of the most important parameters affecting the reflectarray efficiency; therefore it is necessary to study its radiation characteristics properly in order to obtain a valid value for the efficiency. In such cases it is preferred to use a deterministic theoretical model to study the radiation characteristics of the feed antenna. The $\cos^q$ model can be considered the most used mathematical model in this field, due to its simplicity and good results [22]. The radiation pattern of any aperture antenna is expressed — according to $\cos^q$ model — as:

$$RB = 20\log_{10}\log(\cos^q(\theta)) \tag{1}$$

In this study, we use a pyramidal horn antenna with a gain of 12.3 ± 1.5 dB at the frequency band 12–18 GHz. The value of the parameter q that achieves a good agreement between the radiation pattern resulting from Equation (1) and the radiation pattern of the used antenna, resulting from HFSS, as shown in Figure 2, is 7.4. This value of parameter q characterizes the used horn antenna and will be used later to calculate the focal ratio F/D.

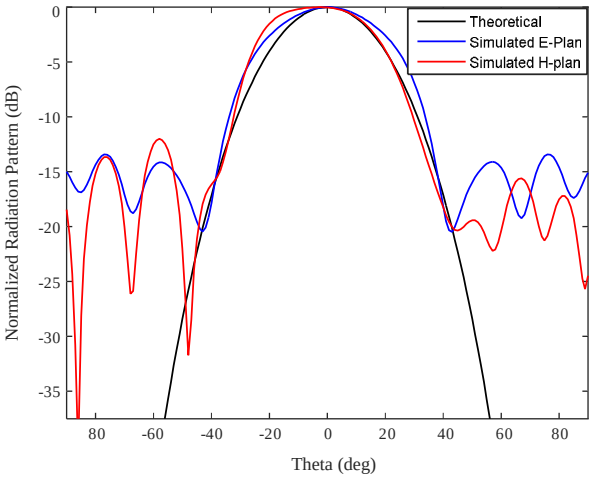

Figure 2. Matching between mathematical and simulation results at the value $q = 7.4$ for the proposed feed antenna.

Deferent researches have studied the appropriate geometry for reflective antennas that depend on spatial feeding in general and for the reflectarray antenna in particular. All these studies have shown that circular shape is the preferred shape that produces the best efficiency for these types of antennas. These results can be roughly justified by observing the projection of the radiation pattern of the feed antenna on an opposite surface at the far field, which is circular.

The diameter of the reflectarray D is directly proportional to its gain and to the design complexity in terms of simulation time and required computational resources. In our design, we chose $D = 250$ mm, and based on this choice and the predetermined value of the parameter q, we calculate the parameter F (which is the distance between the feed antenna and the reflectarray aperture) so that it achieves an acceptable value for the reflectarray efficiency. In theory, the overall reflectarray efficiency is divided into several partial factors, some of which have a significant impact on the total value of the efficiency, and others have a very slight (usually neglected) effect on the total value of the efficiency. The two main factors controlling the total value of the reflectarray efficiency are the illumination efficiency denoted by η_i which is mainly related to the radiation properties of the feed antenna and the parameter q, and the spillover efficiency denoted by η_s which is mainly related to the focal ratio F/D. In this case, the total

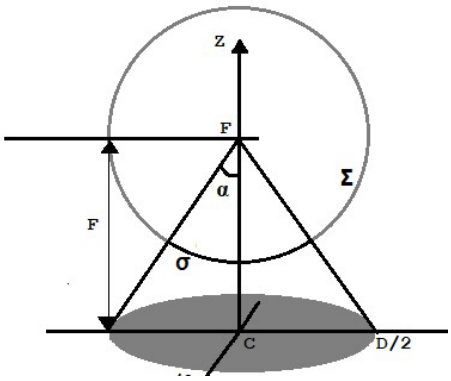

Figure 3. Factors affecting the reflectarray efficiency.

value of the reflectarray efficiency is $\eta_{tot} = \eta_i \eta_s$. According to the studies [3] and [23] and Figure 3, we can write:

$$\eta_i = \frac{4}{\pi D^2} \frac{\left[\int_0^{2\pi}\int_0^{D/2} \frac{1}{r^{1+q_e}} \left(\frac{r_0^2 + r^2 - s^2}{2r_0 r}\right)^q \rho d\rho d\varphi\right]^2}{\int_0^{2\pi}\int_0^{D/2} \frac{1}{r^{2+2q_e}} \left(\frac{r_0^2 + r^2 - s^2}{2r_0 r}\right)^{2q} \rho d\rho d\varphi} \tag{2a}$$

$$\eta_s = \frac{2q+1}{2\pi} \int_0^{2\pi}\int_0^{D/2} \frac{F}{r^3} \left(\frac{r_0^2 + r^2 - s^2}{2r_0 r}\right)^{2q} \rho d\rho d\varphi \tag{2b}$$

where r_0 is the distance between the feed antenna and the center of the reflectarray aperture; r is the distance between the feed antenna and any element on the reflectarray surface; s is the distance between the center of the reflectarray aperture and any element on the reflectarray surface; and q_e is the parameter of the $\cos_q$ model of the reflectarray elements, for simplicity we take $q_e = 1$. Figure 4 results directly from applying the relations in Eqs. (2a) and (2b) in addition to the relationship $\eta_{tot} = \eta_i \eta_s$ using MATLAB. This figure shows the values of (η_{tot}, η_i, and η_s) in terms of the distance between the feed antenna and reflectarray aperture, for $D = 250\,\text{mm}$ and $q = 7.4$, where we notice that the illumination efficiency η_i increases as the distance between the feed antenna and the center of the reflectarray aperture is increased, while the spillover efficiency η_s decreases, so the total efficiency curve goes up to a certain value of F and then starts decreasing, and this value is the optimum value of the distance between the feed antenna and the center of the reflectarray aperture, which is $F = 206\,\text{mm}$ and corresponds to the total efficiency of 77.5% and a focal ratio of 0.824. The total gain of the reflectarray is expressed as:

$$G = D_o * \eta_{tot} = 4\pi \frac{A_e}{\lambda_0^2} \eta_{tot} = \left(\frac{\pi D}{\lambda_0}\right)^2 \eta_{tot} \tag{3}$$

where D_o is the maximum directivity of the reflectarray; A_e is the effective aperture area of the reflective surface whose value is considered to be close to the value of the physical aperture area for the large antennas [24], as in our case; D is the reflectarray diameter; and λ_0 is the free space wavelength at the center frequency of 15 GHz.

The last parameter we study is Edge Taper (ET), which is defined as the ratio of the radiation intensity at the edges of the reflectarray to the maximum radiation intensity in the center of the reflectarray. Consequently, it mainly relates to the specifications and location of the feed antenna and to the focal ratio F/D. Since the electromagnetic waves coming from the feed antenna to the edges of the reflectarray suffer from the diffraction phenomenon, which negatively affects the shape of the radiation pattern of the reflectarray, the value of the ET parameter should be as low as possible (practically less

than $-10\,\text{dB}$). The parameter ET is given:

$$ET = 20\log_{10}\left(\frac{2F}{D}\sin(\alpha)\cos^{q}(\alpha)\right) \tag{4}$$

where α is the feed subtended angle within which the illumination varies from a maximum value at the center, to a minimum value at the edge. Mathematically, we get the value $ET = -11.4366\,\text{dB}$, which is practically acceptable.

3. PHASE DISTRIBUTION FORMULATION OF THE DIFFERENT CONCENTRATED ZONES ON THE REFLECTARRAY SURFACE

The reflectarray antenna is composed of a reflective surface with relatively big diameter and a feed antenna relatively far from it as shown in Figure 1. Therefore, the electromagnetic waves coming to each radiating element on the reflectarray surface suffer from different not-neglected time delays, and hence not-neglected phase differences. These time delays should be compensated in order to obtain in-phase reflected waves in the far field of the reflectarray, thus achieving a main lobe with high gain and narrow beamwidth. For this purpose, the TTD technique that includes calculating the required phase distribution on the reflectarray surface is studied.

Since the effective aperture of the used feed antenna is less than 50 mm, and since the diameter of the studied reflective surface is 250 mm, the effective aperture of the used feed antenna to the diameter of the studied reflective surface ratio is less than 0.2; the disadvantages of the feed blockage are negligible [3]; and there is no need to use the shifted-fed design.

Since the reflectarray under study is center-fed and circular aperture, there are regions on the reflectarray surface (circular rings around the center of the reflectarray) in which the phase delays are equal. Therefore, the reflectarray surface can be divided into a number of concentric zones (circular rings of equal width), so that the unit cells in each of these zones are completely identical, as shown in Figure 5 [20]. The number of zones is a design parameter that results in a quantization error; the bigger the number of zones is, the smaller the quantization error is, but the more design complexity and the more difficult to manufacture, and on the other hand, the smaller the number of zones is, the greater the quantization error is which affects the reflectarray performance. The width of each zone is usually determined to accommodate at least one unit cell, and then the number of zones is calculated by knowing the reflectarray diameter and the dimensions of the unit cell.

Using sub-wavelength technique to design unit cells with dimensions less than half-wavelength increases the number of radiating elements on the reflectarray surface and their proximity to each other, which leads to the generation of resonance coupling between them, and thus the ability to modify

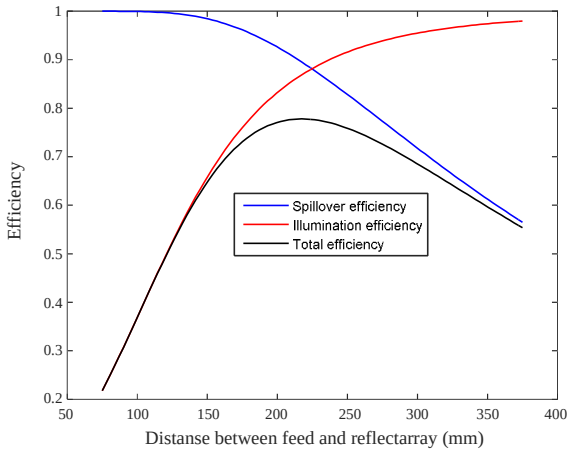

Figure 4. Reflectarray efficiencies for $D = 250\,\text{mm}$ and $q = 7.4$.

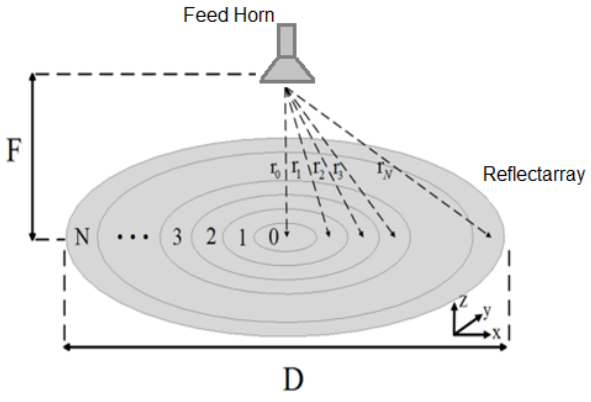

Figure 5. The time delays of the electromagnetic waves at each zone on the reflectarray surface.

the reflection coefficient phase for the radiating element as required. However, this technique can lead to a decrease in the phase range of the radiating elements due to their small dimensions, and thus reduce the overall efficiency of the reflectarray. In our design we did not use the sub-wavelength technique, so the dimensions of the unit cell are equal to the half-wavelength of the free-space at the center frequency, i.e., $d = 10\,\text{mm}$. By specifying the width of each zone so that it accommodates one unit cell and taking into account the diameter of the reflectarray aperture, the number of zones is determined to be $N = 13$. The next step is to calculate the phase distributions required to compensate for time delays in each zone.

As we mentioned earlier, the electromagnetic fields spread from the feed antenna towards the radiating elements of the reflectarray with different time delays, and thus with different phase delays. Therefore, these radiating elements must be designed in certain shapes or sizes so that they compensate the different phase delays, which results in the formation of a focused beam in the desired direction (in our case the broadside direction). The distance between the feed antenna and the center of the ith zone of reflectarray aperture is r_i as shown in Figure 5, hence, the corresponding phase delay in this zone is given by $\phi_{pd}^{(i)} = -k_0 r_i$, where $k_0 = 2\pi/\lambda_0$ is the propagation constanat of the free space. Assuming that the distance between the center of the reflectarray and the center of the ith zone of reflectarray aperture is d_i, then $r_i = \sqrt{F^2 + d_i^2}$. Thus the phase delay at the center of the ith zone is given by:

$$\phi_{pd}^{(i)} = -\frac{2\pi}{\lambda_0}\sqrt{F^2 + d_i^2} \tag{5}$$

To compensate this phase delay, the required phase distribution in the ith zone of the reflectarray aperture is given by:

$$\phi_{RA}^{(i)} = \frac{2\pi}{\lambda_0}\sqrt{F^2 + d_i^2} = \frac{2\pi}{c}\left(\sqrt{F^2 + d_i^2}\right) f \tag{6}$$

where $i = 1 \ldots N$ is the zone index. Equation (6) represents the optimal phase distribution required in each zone to form the desired focused beam. By applying Equation (6) in practice, we obtain several ascending linear curves in terms of frequency representing the reflection coefficient phase in each zone. But knowing that the reflection coefficient phase of the reflectarray elements is a descending function with the frequency (according to the results of the next section), Equation (6) must be modified to match the practical results without affecting the phase distribution of the different zones. One modification method is to consider the phase provided by the last zone of the reflectarray as a reference phase to be subtracted from all phases of the different zones, as follows:

$$\phi_{RA}^{(i)} = \frac{2\pi}{c}\left(\sqrt{F^2 + d_i^2} - \sqrt{F^2 + d_N^2}\right) f + \pi \tag{7}$$

where d_N is the distance between the center of the reflectarray and the center of the Nth zone of reflectarray aperture. Since we have chosen to design the unit cells equal to the half-wavelength of the free space, these unit cells will be resonant at the frequency corresponding to the half-wavelength of the free space. If the physical length is $\lambda_0/2$, then the electrical length is $\beta l = (2\pi/\lambda_0)(\lambda_0/2) = \pi$, thus the resonance frequency of the unit cells in each zone is the frequency corresponding to a reflection coefficient phase equal to an odd integer of π. To take advantage of the resonant properties of the radiating elements, they must resonate at the fundamental harmonic ($f = 0$), which is why we added a fixed phase π to Equation (7).

The last step is to return all the curves to the desired operating frequency band [12–18 GHz], which is done by adding an integer of 2π to the curves that need it, as follows:

$$\phi_{RA}^{(i)} = \frac{2\pi}{c}\left(\sqrt{F^2 + d_i^2} - \sqrt{F^2 + d_N^2}\right) f + \pi + 2\pi m \tag{8}$$

Since this addition is an integer of 2π, it will not affect the phase distribution of the different zones. The reflection coefficient phases of different zones within the desired operating frequency band [12–18 GHz], which must be achieved when the unit cells are designed in each zone, are shown in Figure 6.

Table 1 shows the phase range required by the radiating elements at different frequencies to be able to achieve the phase distributions shown in Figure 6 which must be taken into account when the unit cells are designed in each zone.

Table 1. The phase range required by the radiating elements at different frequencies.

Frequency	Required phase range
12 GHz	$[-169.57^\circ\ 130.14^\circ] = 299.71^\circ$
13 GHz	$[-198.70^\circ\ 95.98^\circ] = 294.68^\circ$
14 GHz	$[-254.05^\circ\ 61.83^\circ] = 315.88^\circ$
15 GHz	$[-310.77^\circ\ 27.67^\circ = 338.44^\circ$
16 GHz	$[-367.49^\circ\ -6.49^\circ] = 361.00^\circ$
17 GHz	$[-424.20^\circ\ -40.64^\circ] = 383.56^\circ$
18 GHz	$[-480.92^\circ\ -74.80^\circ] = 406.13^\circ$

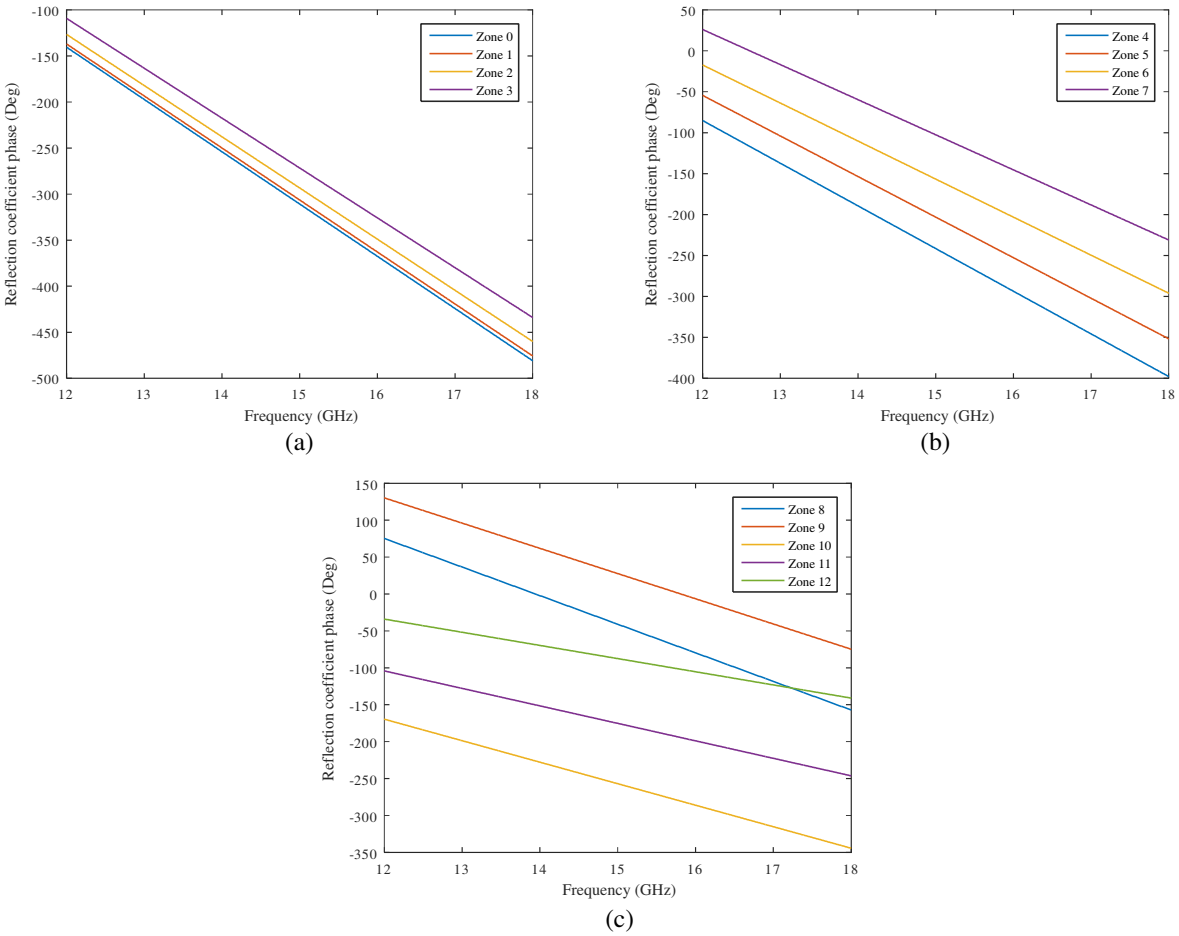

Figure 6. The reflection coefficient phases of different zones within the desired operating frequency band.

4. UNIT CELL DESIGN USING FSS CONFIGURATION AND EQUIVALENT CIRCUIT MODEL

The final goal in the unit cell design stage is to find the appropriate physical dimensions for the unit cells in each zone that achieve the phase distributions produced in the previous section (Figure 6). In the following, we will rely on the unit cell analysis methodology that includes the following steps:

- Propose an appropriate FSS configuration that fulfills the design requirements (specific filtering properties, specific radiation properties, specific frequency range, specific phase range ...).
- Extract the equivalent circuit model for the selected FSS configuration.
- Find mapping between the electrical values of the equivalent circuit and the physical values of the FSS configuration.
- Analyze the unit cell using numerical analysis software to optimize its performance.

Generally, the chosen FSS configuration should achieve the following features:

- The changes in the physical dimensions of the proposed FSS configuration must achieve a sufficient phased range so that they are able to compensate the various phase delays of the electromagnetic fields generated from the feed antenna.
- It is desirable that the proposed configuration being symmetrical achieving this condition ensures good performance of the RA in both E- and H-planes.
- To ensure the linear phase of the reflection coefficient over the entire frequency range, and therefore the design of wideband reflectarrays, it is necessary to either choose a single-layer complex configuration, or choose a multi-layer simple configuration to increase the degrees of freedom.

For this research, we choose an FR4 substrate with dielectric constant of 4.4 and loss tangent of 0.02 to design the reflectarray elements. It is worth pointing out that the dielectric substrate type and thickness have a significant impact on the reflection coefficient phase for different FSS configurations. Generally, the frequency range of the radiating elements increases with the thickness of the used dielectric substrate, but this leads to the difficulty of achieving a sufficient phase range for these elements, and vice versa. As we mentioned before, to ensure the linear phase of the reflection coefficient over the entire frequency range, it is necessary to either choose a single-layer complex configuration or choose a multi-layer simple configuration. In this research, we prefer that the configuration is multi-layer and simple to reduce the degrees of freedom and thus simplify the simulation and tuning operations on the one hand, and to simplify the process of extracting the equivalent circuit model on the other hand.

Table 2 shows the phase ranges of six simple FSS configurations, and the expected fractional frequency range for each of them, for the thickness $t = 0.33\,\text{mm}$ of the dielectric substrate. The proposed configurations were analyzed using HFSS software, where the unit cell is treated as an infinite array of identical unit cells. We notice from Table 2 that the two layers with square loop shape is the simplest FSS configuration that achieves sufficient phase range over the entire Ku-band for the FR4 dielectric substrate.

Table 2. The frequency and phase ranges of six simple FSS configurations.

Phase range	Square patch		Square aperture		Square loop	
	One layer	Two layers	One layer	Two layers	One layer	Two layers
At 12 GHz	166.14°	359.70°	96.43°	180.79°	350.84°	357.41°
At 13 GHz	150.68°	347.53°	112.49°	244.32°	270.67°	443.12°
At 14 GHz	136.20°	317.10°	130.97°	302.16°	274.12°	487.24°
At 15 GHz	122.78°	283.32°	151.81°	344.59°	281.41°	490.38°
At 16 GHz	110.39°	246.63°	174.51°	409.94°	337.88°	492.36°
At 17 GHz	98.98°	209.94°	197.89°	431.59°	337.04°	501.68°
At 18 GHz	88.50°	176.62°	220.59°	447.47°	308.20°	538.68°
Expected FBW	**0**	**10%**	**0**	**15%**	**6.7%**	**40%**

Table 3 shows the phase ranges of the two layers with square loop FSS configuration with three different thicknesses of the FR4 dielectric substrate, and the expected fractional frequency range for each case. The proposed configurations were analyzed using HFSS, where the unit cell is treated as an

Table 3. The effect of the substrate thickness on the frequency and phase ranges.

Phase range	$t = 0.33$ mm	$t = 1$ mm	$t = 1.6$ mm
At 12 GHz	357.41°	351.35°	354.28°
At 13 GHz	443.12°	358.04°	349.54°
At 14 GHz	487.24°	368.27°	340.38°
At 15 GHz	490.38°	455.89°	350.45°
At 16 GHz	492.36°	521.08°	193.63°
At 17 GHz	501.68°	503.87°	118.21°
At 18 GHz	538.68°	507.08°	54.24°
Expected FBW	**40%**	**40%**	**20%**

infinite array of identical unit cells. We notice from Table 3 that by increasing the thickness of the used dielectric substrate, both the phase and frequency ranges of the radiating elements decrease.

In the two layers with a square loop FSS configuration shown in Figure 7(a), the straight arm of the square-loop in each layer can be represented by an inductor L, and the distance between two adjacent square-loops on each layer can be represented by a capacitor C. Consequently, the equivalent circuit model of the two-layer square-loop FSS configuration is a two-stage low pass filter. The frequency normalization equations are then applied to obtain the two-stage band stop filter, thus moving to the desired frequency band. Finally, the parallel branches of the band stop circuit are replaced by admittance inverters to ensure that the radiating elements are practicable with printed circuit technology, where these inverters are represented physically by $\lambda_0/4$ transmission lines at center frequency [24]. The modified circuit of the band stop filter after adding the admittance inverters is shown in Figure 7(b), and the equivalent circuit model of the unit cell after adding the $\lambda_0/4$ transmission lines is shown in Figure 7(c).

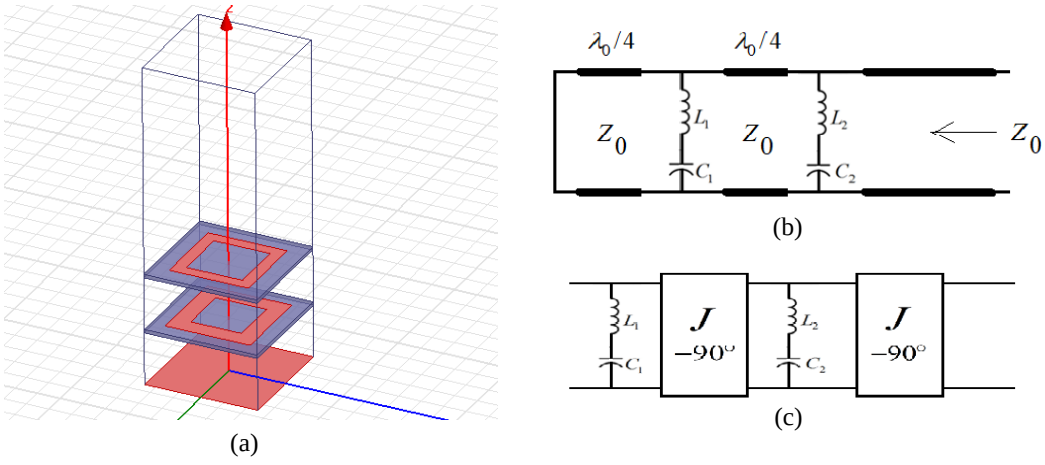

Figure 7. Two-layer square-loop unit cell. (a) The physical model, (b) the modified band pass circuit after adding the admittance inverters, and (c) the equivalent circuit model after adding the $\lambda_0/4$ transmission lines.

Mathematically, the values of the inductors and capacitors required to obtain the desired phase distribution can be calculated from the following equation [24]:

$$L_{n,i} = \frac{T_i f_c Z_0}{2\ B(2n-1)} \tag{9a}$$

$$C_{n,i} = \frac{2\ B(2n-1)}{T_i f_c f_i^2 Z_0 (4\pi)^2} \tag{9b}$$

where B is the bandwidth of the antenna under study (i.e., $B = 6\,\text{GHz}$); T_i is the reflection coefficient phase slope in each zone i obtained from Figure 6; f_i is the resonance frequency of the unit cells in each zone i obtained also from Figure 6; f_c is the bandwidth of the low pass circuit; and n is the layer index (i.e., $n = 1, 2$). By applying Eq. (9), we obtain the values of the inductors and capacitors for unit cells in each zone of the reflectarray surface, shown in Table 4.

The final step in the unit cell design process is to calculate the physical dimensions of the radiating elements in each zone and each layer depending on the corresponding LC values, so that an acceptable

Table 4. LC values for unit cells in each zone.

zone	First layer		Second layer	
	L_1 (nH)	C_1 (fF)	L_2 (nH)	C_2 (fF)
0	4.37	36	13.1	12
1	4.34	35.82	13.03	11.94
2	4.28	35.27	12.83	11.76
3	4.16	34.35	12.5	11.45
4	4.01	33.08	12.03	11.03
5	3.81	31.45	11.44	10.48
6	3.58	29.49	10.73	9.83
7	3.3	27.19	9.89	9.06
8	2.98	24.59	8.94	8.2
9	2.63	86.73	7.89	28.9
10	2.24	73.97	6.73	24.7
11	1.82	60.14	5.47	20
12	1.37	45.29	4.12	15.1

Table 5. The final physical dimensions of the radiating elements in each zone and each layer.

zone	First layer		Second layer	
	L_1 (mm)	W_1 (mm)	L_2 (mm)	W_2 (mm)
0	4.99	1	4.63	0.32
1	4.98	1	4.63	0.32
2	5.2	1	4.32	0.31
3	5	1	4.32	0.38
4	5.07	1	3.85	0.4
5	4.8	1	3.05	0.4
6	4.15	1.5	0.8	0.25
7	1.6	0.25	9.8	0.25
8	5.28	2	5.55	0.4
9	7.25	1.31	4.29	0.35
10	9.24	4.3	2	0.25
11	6.3	2.9	0.8	0.25
12	9.8	4.7	9.8	1.5

match is obtained for the reflection coefficient curves resulting from both the electrical and physical models. The study [25] presents a set of experimental equations to calculate the dimensions of the square-loop type FSS shown in Figure 7(a) based on the LC values and the specifications of the used dielectric substrate. However, since these equations are experimental and may produce inaccurate results, the resulting values need some tuning to give the required performance.

The physical dimensions of the radiating elements in each zone and each layer, after tuning, are shown in Table 5. The reflection coefficient phases of the unit cells of different zones for both physical (Figure 7(a)) and theoretical (Equation (8)) designs are shown in Figure 8, where an acceptable match between the corresponding curves is observed, and thus the final goal in the unit cell design stage is achieved.

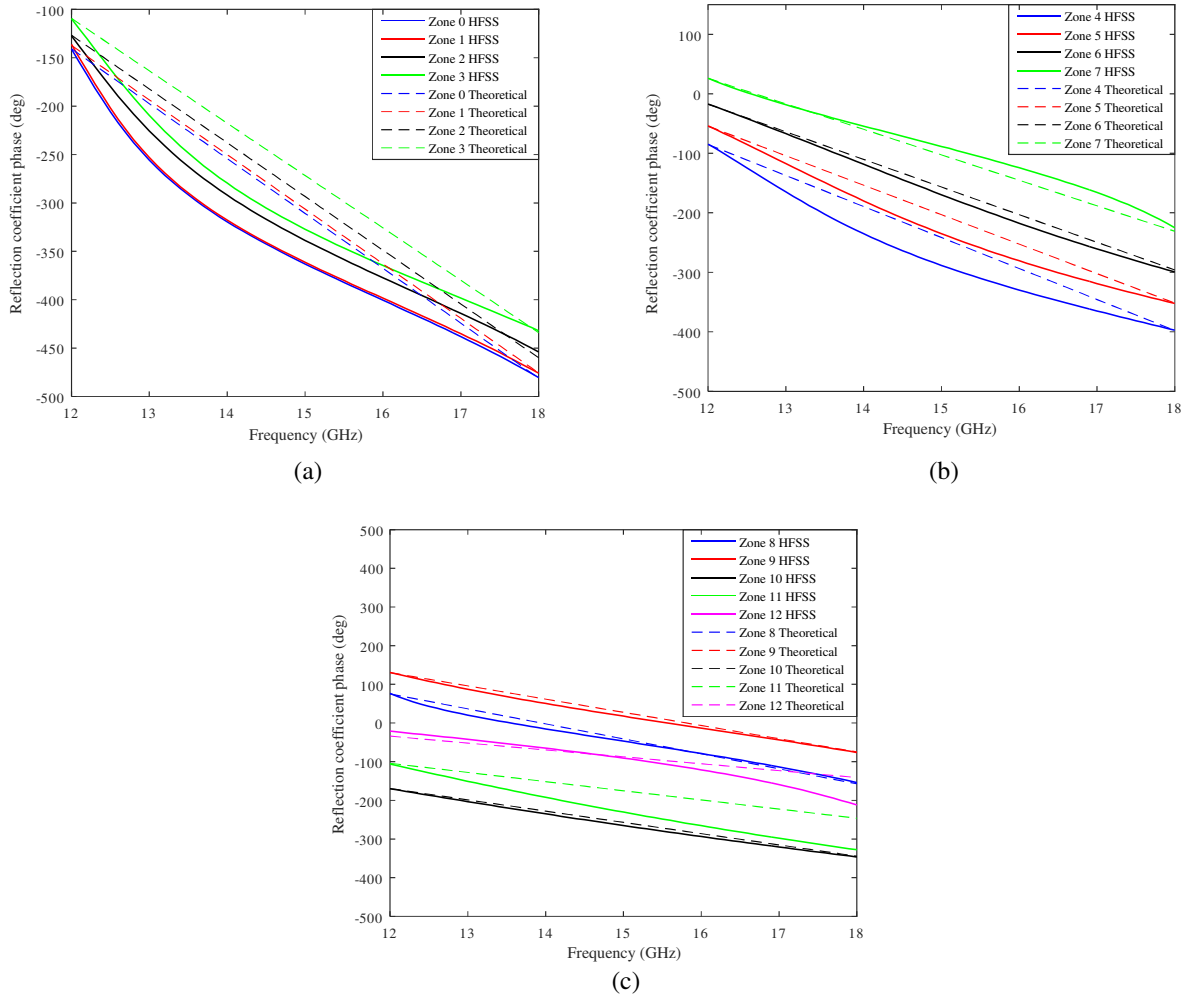

Figure 8. The reflection coefficient phase of the unit cells of different zones for both physical and electrical designs.

5. REFLECTARRAY ANTENNA DESIGN AND SIMULATION

In Section 2, the basic parameters of the reflectarray under study are presented (the reflective surface diameter, the feed antenna specifications, location, distance from the reflectarray, and the reflective surface shape). In Section 3, the TTD technique is applied to the reflectarray under study (the different zones of the reflective surface and the phase distribution in each zone). In Section 4, the unit cell parameters are presented (the proposed FSS configuration, the number of layers, and the physical

dimensions of unit cells in different zones and layers). Accordingly, the design of the reflectarray antenna can be achieved.

The large number of RA elements (517 elements) and their positioning in different locations and different dimensions according to their locations made the design process on HFSS complex and required a lot of time, effort, and focus, with a high probability of error. This prompted us to search for a more effective, easy, and reliable way to design the required RA antenna. HFSS allows linking the 3D design with the visual basic language. This feature was used to programmatically implement the RA circuit and then link the code with HFSS, which greatly simplified the design process.

The entire configuration (consisting of the reflectarray antenna and the feed antenna) is designed using HFSS software as shown in Figure 9, with the adoption of the Finite Element-Boundary Integration (FE-BI) solution method which gives very good results with less consumption of time and computer resources. The FE-BI method is a hybrid method that combines the advantages and addresses the disadvantages of the Finite Element Method (FEM) and the Integral Equation method (IE).

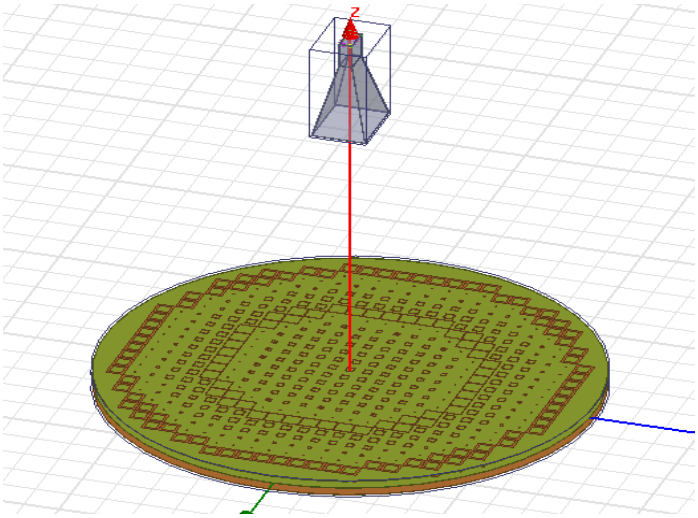

Figure 9. The reflectarray with the feed antenna designed using HFSS.

The normalized co- and cross-polarized radiation patterns in the far field of the designed reflectarray in both E and H planes, at the frequencies 12, 15, and 18 GHz are shown in Figure 10. We notice from Figure 10 that the designed reflectarray provides a focused beam in the desired direction with a value of HPBW less than 6 degrees in both E and H planes at the frequencies 12, 15, and 18 GHz. We also notice that the side-lobes are less than -1 dB in both E and H planes at the frequencies 12, 15, and 18 GHz. Figure 10 also shows that the level of the cross-polarized radiation is less than the level of the co-polarized radiation by approximately 40 dB in both E and H planes at the frequencies 12, 15, and 18 GHz.

Figure 11 shows both the simulation gain and theoretical gain (taking into account the spillover and illumination efficiencies only, this theoretical gain was calculated from Equation (3)) of the reflectarray antenna in the desired direction and over the entire studied frequency band (Ku-band), where it is observed that the simulation gain is 26.77 dB at the center frequency of 15 GHz with gain variations less than 1.5 dB within the Ku-band, achieving a fractional bandwidth of 40%, and considering that the fractional bandwidth of the used horn antenna is 40%, the proposed RA antenna provides maximum fractional bandwidth.

Figure 11 also shows that the theoretical gain values are bigger than the simulation ones. These differences can be justified by the phase efficiency that is one of the important parameters that affect the total efficiency of the reflectarray antenna. The phase efficiency can be calculated by comparing the values of theoretical gain and simulated gain in Figure 11.

Figure 12 shows the phase efficiency of the proposed RA antenna over the entire Ku-band. The

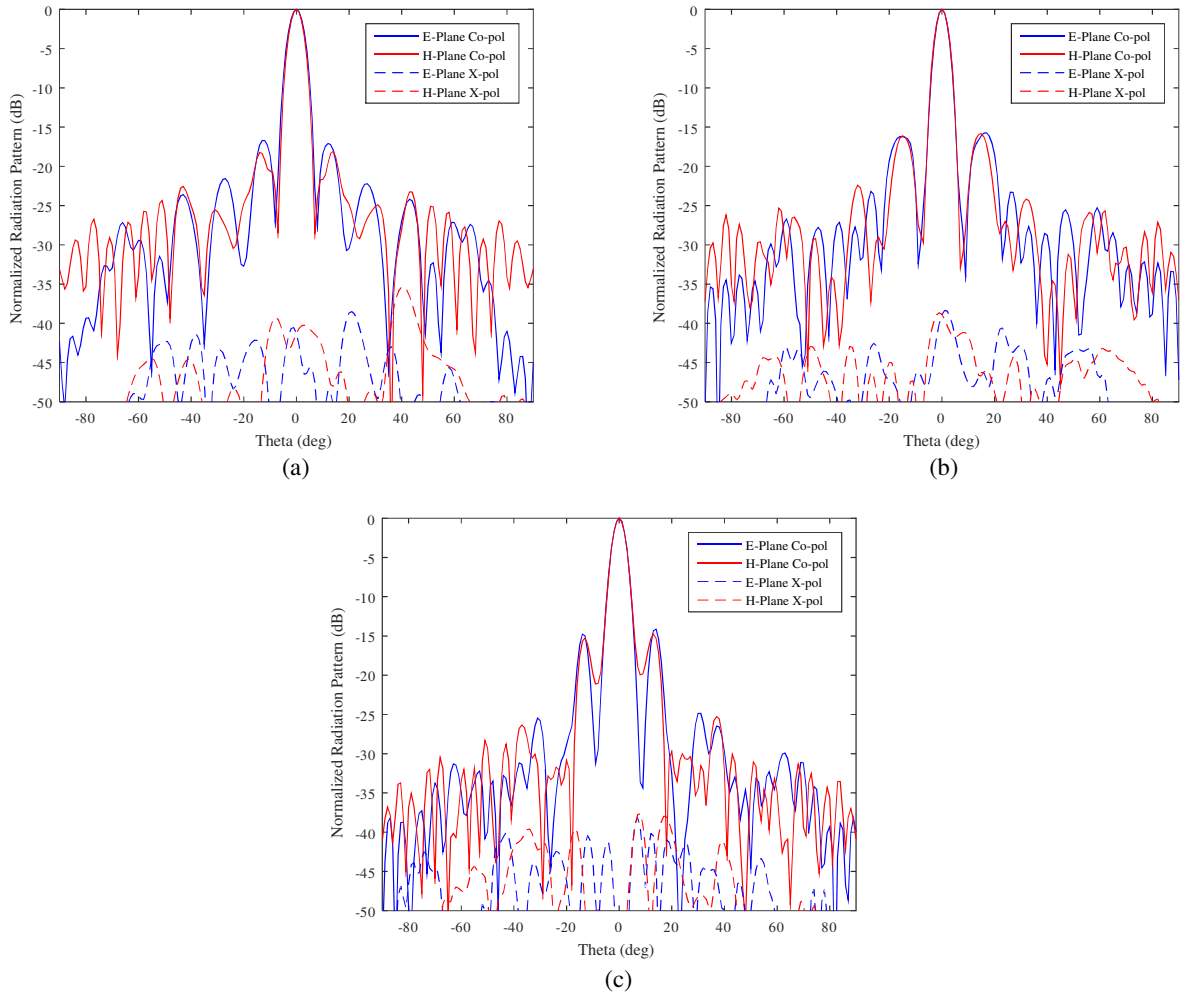

Figure 10. Normalized co- and cross-polarized radiation patterns of the proposed reflectarray. (a) $f = 12\,\text{GHz}$, (b) $f = 15\,\text{GHz}$, (c) $f = 18\,\text{GHz}$.

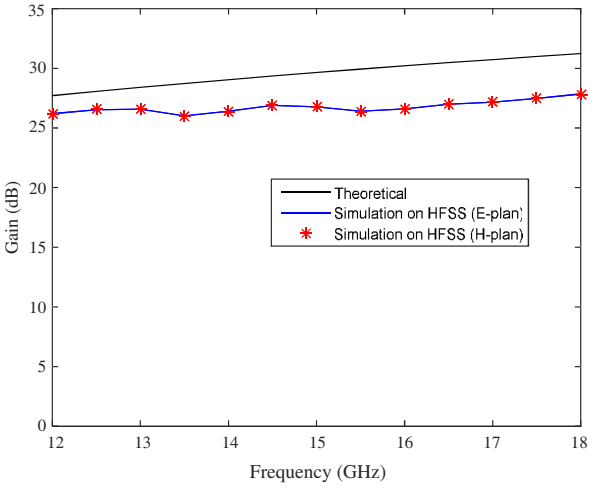

Figure 11. Theoretical and simulation gain of the proposed reflectarray antenna.

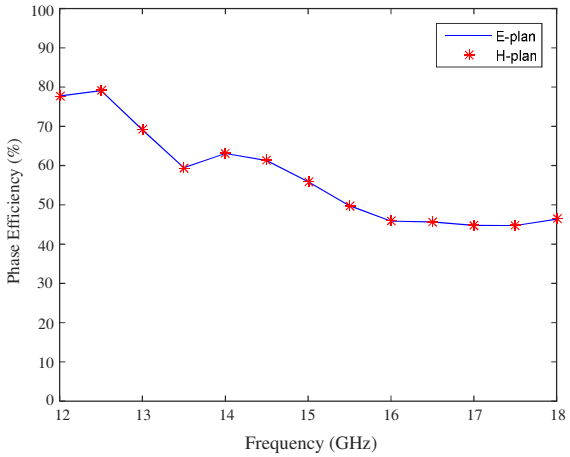

Figure 12. Phase efficiency of the proposed RA over the entire Ku-band.

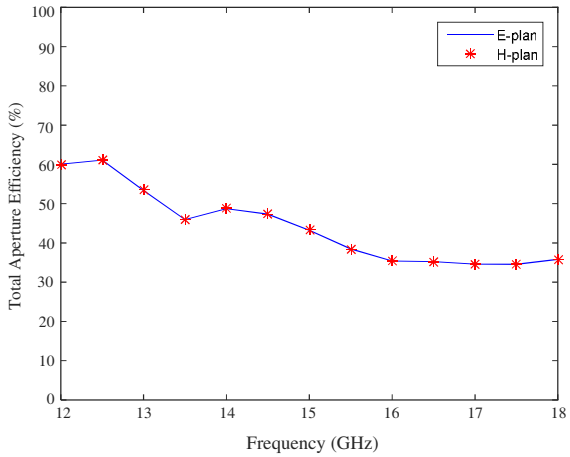

Figure 13. The total efficiency of the proposed RA over the entire Ku-band.

phase efficiency mainly results from the approximations occurring during the phase compensation process that can be seen through the mismatch of the theoretical and practical phase distribution curves over the entire frequency range studied in Figure 8, and this explains the low values of the phase efficiency at some frequencies.

By adding the effect of the phase efficiency to the total efficiency, we can calculate the value of the new total efficiency of the RA antenna using the following equation:

$$\eta_{total} = \eta_i \eta_s \eta_{ph} \tag{9c}$$

where η_{total} is the phase efficiency. Figure 13 shows the final total efficiency of the proposed RA antenna over the entire Ku-band.

6. EXPERIMENTAL VERIFICATION AND MEASUREMENT RESULTS

A prototype of the wideband reflectarray antenna was fabricated as shown in Figure 14. The proposed reflectarray antenna is composed of two main layers with a ground. Each of the two main layers is composed of an FR4 substrate with dielectric constant of 4.4, loss tangent of 0.02, thickness of 0.33 mm, and numerous square-loop radiating elements placed on top of it. The dimensions of the radiating

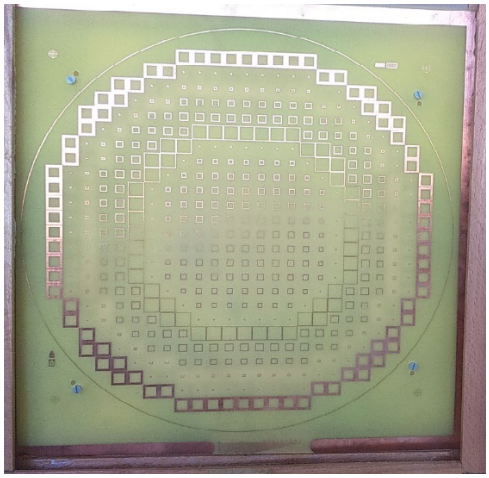

Figure 14. The fabricated reflectarray antenna.

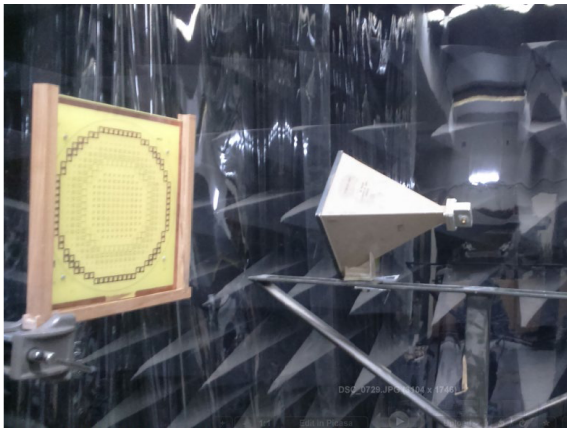

Figure 15. The measurement process of the fabricated reflectarray antenna in anechoic chamber.

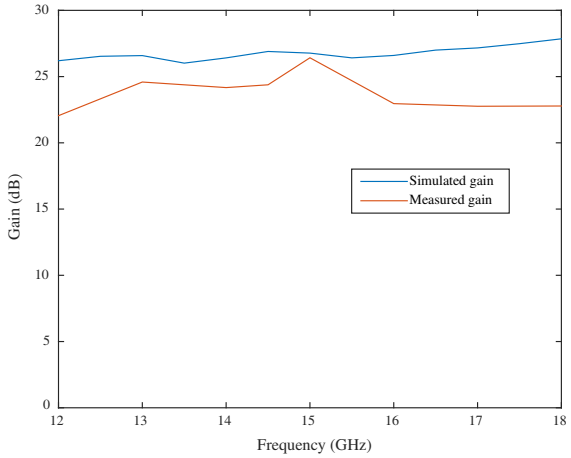

Figure 16. The simulated and measured gains of the proposed reflectarray antenna.

Table 6. A comparison of our reflectarray with other works in the literature.

Ref.	Unit cell configuration	Design technique	Aperture size (λ_0)	Num. of unit cells	Center frequency (GHz)	Gain at center frequency (dB)	Side-lobe level (dB)	Cross-pol. level (dB)	FBW (%)
[13]	Single-layer Cross loop and square ring slot loaded patch	Not TTD Not sub-wavelength	14×14	324	14	23	< -10	< -40	50.75 (3-dB)
[15]	Two-layers Grounded loop-wire	Not TTD sub-wavelength	8.7×8.7	524	10	26	< -15	-25	25 (3-dB)
[16]	Two-layers Two concentric circular rings	Not TTD sub-wavelength	10×10	648	10	26.26	—	—	27.5 (1.5-dB)
[18]	Two-layers Rectangular-shaped patches	TTD Not sub-wavelength	27×27	1888	10	36.3	< -20	< -30	26.7 (1.5-dB)
[19]	Two-layers Rectangular-shaped patches	TTD sub-wavelength	7.8×7.8	1129	10	23.7	< -10	< -10	40 (3-dB)
[20]	Two-layers Dog-bone type	TTD Not sub-wavelength	16.7×16.7	960	10	29.7	-20	< -40	40 (1.5-dB)
This work	Two-layers Square-loop type	TTD Not sub-wavelength	12.5×12.5	517	15	26.42	< -15	< -40	40 (2-dB)

elements in both main layers are taken from Table 5, and the diameter of the resulted reflectarray antenna is 250 mm. The used feed antenna is a pyramidal horn antenna with a gain of 12.3 ± 3 dB at the frequency band 12–18 GHz and is placed in front of the reflective surface so that it achieves the focal ration $F/D = 0.824$.

The maximum gain of the fabricated reflectarray antenna was measured at different frequencies within the Ku-band antenna in an anechoic chamber as shown in Figure 15.

Figure 16 shows the simulated and measured gains of the proposed reflectarray antenna. As seen, there is a good agreement between the simulated and measured results within the Ku-band.

A comparison of our work with other works in the literature is presented in Table 6, where it is observed that our design produces good radiation properties with smaller aperture size, fewer unit cells, dielectric substrate with less performance, and simpler unit cell configuration.

7. CONCLUSION

A true-time-delay ultra-wideband reflectarray antenna operating in Ku-band is studied, analyzed, and designed. Different parameters affecting the efficiency of the reflectarray, including the specifications of the feed antenna, have been studied. The phase distribution in the different zones of the reflectarray surface was calculated. The appropriate FSS configuration for the design of the unit cells in each zone of the reflectarray surface has been studied and selected, and the appropriate number of layers that achieves the required phase distribution of the unit cells in each zone has been chosen. The equivalent circuit model of the selected FSS configuration has been studied. The LC values of the equivalent circuit model that achieve the required phase distribution in each zone have been calculated, and accordingly, the physical dimensions of the FSS configuration in each zone were calculated. A reflectarray antenna with a horn antenna for feeding is designed to operate at the center frequency of 15 GHz. The practical results indicate that the reflectarray radiation properties are relatively consistent within the frequency band 12–18 GHz, achieving a fractional bandwidth of 40%.

ACKNOWLEDGMENT

This work has been supported by the Higher Institute for Applied Sciences and Technology (HIAST).

CONFLICT OF INTEREST

The authors declare no conflict of interest.

REFERENCES

1. Huang, J. and J. A. Encinar, *Reflectarray Antennas*, John Wiley & Sons, Inc., 2008.
2. Munk, B., *Finite Antenna Arrays and FSS*, Wiley, New York, 2003.
3. Nayeri, P., F. Yang, and A. Z. Elsherbeni, *Reflectarray Antennas: Theory, Designs, and Applications*, John Wiley & Sons, Inc., 2018.
4. Narayan, S., B. Sangeetha, and R. M. Jha, *Frequency Selective Surfaces Based High Performance Microstrip Antenna*, Springer, Singapore, 2016.
5. Munk, B., *Frequency Selective Surfaces*, John Wiley & Sons, Inc., New York, 2000.
6. Liang, L. and S. V. Hum, "Design of a UWB reflectarray as an impedance surface using bessel filters," *IEEE Trans. Antennas Propagat.*, Vol. 64, No. 10, 4242–4255, Oct. 2016.
7. Bodur, H., S. Ünaldi, S. Çimen, and G. Çakir, "A novel reflectarray antenna combined with double layer FSS for RCS reduction," *Proc. 25th Telecommun. Forum (TELFOR)*, 1–3, Nov. 2017.
8. Momeni Hasan Abadi, S. M. A., K. Ghaemi, and N. Behdad, "Ultra-wideband, true-time-delay reflectarray antennas using ground-plane-backed, miniaturized-element frequency selective surfaces," *IEEE Trans. Antennas Propagat.*, Vol. 63, No. 2, 534–541, Feb. 2015.

9. Li, H., B. Z. Wang, G. Zheng, and W. Shao, "A Reflectarray antenna backed on FSS for low RCS and high radiation performances," *Progress In Electromagnetics Research C*, Vol. 15, 145–155, 2010.
10. Fakharian, M. M., P. Rezaei, and A. A. Orouji, "A Reflectarray based on the folded SIR patch-slot configuration backed on FSS for low RCS," *Progress In Electromagnetics Research Letters*, Vol. 47, 119–124, 2014.
11. Zhong, X., H.-X. Xu, L. Chen, W. Li, H. Wang, and X. W. Shi, "An FSS-backed broadband phase-shifting surface array with multimode operation," *IEEE Trans. Antennas Propag.*, Vol. 67, No. 9, 5974–5989, Sep. 2019.
12. Wu, G., S. Qu, Y. Wang, and S. Yang, "Nonuniform FSS-backed reflectarray with synthesized phase and amplitude distribution," *IEEE Trans. Antennas Propag.*, Vol. 66, No. 12, 6883–6892, Dec. 2018.
13. Lingasamy, V., M. Gulam Nabi Alsath, K. T. Selvan, and R. Jyoti, "A wideband, single layer reflectarray antenna with cross loop and square ring slots loaded patch elements," *International Journal of Microwave and Wireless Technologies*, Vol. 11, No. 7, 703–710, Sep. 2019.
14. Edalati, A. and K. Sarabandi, "Wideband reflectarray antenna based on miniaturized element frequency selective surfaces," *Proc. Eur. Conf. Antennas Propag. (EuCAP2012)*, 362364, 2012.
15. Edalati, A. and K. Sarabandi, "Reflectarray antenna based on grounded loop-wire miniaturised-element frequency selective surfaces," *IET. Microw. Antennas Propag.*, Vol. 8, No. 12, 973–979, Sep. 2014.
16. Nourinia, J., et al., "RCS reduction of reflectarray antenna backed with sub-wavelength frequency selective surface," *2019 27th Iranian Conference on Electrical Engineering (ICEE)*, 1627–1631, IEEE, 2019.
17. Momeni Hasan Abadi, S. M. A. and N. Behdad, "Design of wideband, FSS-based multi-beam antennas using the effective medium approach," *IEEE Trans. Antennas Propag.*, Vol. 62, No. 11, 5557–5564, Nov. 2014.
18. Carrasco, E., J. A. Encinar, and M. Barba, "Bandwidth improvement in large reflectarrays by using true-time delay," *IEEE Trans. Antennas Propagat.*, Vol. 56, No. 8, 24962503, Aug. 2008.
19. Momeni Hasan Abadi, M. A. and N. Behdad, "Broadband true-time-delay circularly polarized reflectarray with linearly polarized feed," *IEEE Trans. Antennas Propag.*, Vol. 64, No. 11, 4891–4896, Nov. 2016.
20. Delafkar, H., A. Pirhadi, and S. Karimian, "A new model for design of wideband radiating elements for reflectarray antenna," *2017 IEEE Asia Pacific Microwave Conference (APMC)*, 73–76, IEEE, 2017.
21. Legay, H., D. Bresciani, E. Labiole, R. Chiniard, and R. Gillard, "A multi facets composite panel reflectarray antenna for a space contoured beam antenna in Ku band," *Progress In Electromagnetics Research B*, Vol. 54, 1–26, 2013.
22. Stutzman, W. L. and G. A. Thiele, *Antenna Theory and Design*, John Wiley & Sons, Inc., 2012.
23. Yu, A., F. Yang, A. Z. Elsherbeni, J. Huang, and Y. Rahmat-Samii, "Aperture efficiency analysis of reflectarray antennas," *Microw. Opt. Technol. Lett.*, Vol. 52, No. 2, 364–372, Feb. 2010.
24. Pozar, D. M., *Microwave Engineering*, John Wiley & Sons, Inc., 2009.
25. Xu, Y. and M. He, "Design of multilayer frequency-selective surfaces by equivalent circuit method and basic building blocks," *International Journal of Antennas and Propagation*, 1–13, 2019.